An Efficient Digital Backend for Wideband Single-Carrier mmWave Massive MIMO

Mohammed Abdelghany, Upamanyu Madhow, *Fellow, IEEE*, and Mark Rodwell, *Fellow, IEEE*.

***Abstract*—Millimeter wave (mmWave) carrier frequencies offer the dual benefits of large bandwidth and physically compact antenna arrays with a large number of elements, so that a large number of simultaneous independently modulated users can be supported with digital beamforming. In this paper, we propose an efficient digital backend design for a wideband mmWave massive MIMO uplink taking full advantage of both features. The challenges in receiver design for a wideband system with a large antenna array include the following: (a) for each user, there is a multi-symbol delay spread across the array, hence the receiver must handle intersymbol as well as multiuser interference; (b) even though we consider channels with a single dominant path, the spatial frequency for a user becomes smeared across the band; (c) the natural strategy of MIMO-OFDM used at lower carrier frequencies is unattractive at mmWave frequencies because the linearity requirements due to large peak-to-average ratio are difficult to meet. In this paper, we introduce a novel technique that combines spatial domain FFT and time-domain FFT, together with an interpolation technique for limiting the spread of spatial frequency across the band which significantly reduces the complexity of beamformer weight acquisition. We present simulation results for a system operating at 140 GHz with a bandwidth of 14 GHz and a 256-element horizontally-scanning linear base station array.**

Keywords*—*LMMSE, single-carrier, wideband, uplink massive MIMO system.

I. Introduction

We consider an all-digital mmWave massive MIMO uplink that takes advantage of the following key characteristics of mmWave frequencies: massive available bandwidth, compact antenna arrays with a large number of elements, and digital beamforming for supporting a large number of simultaneous users, scaling with the number of antenna elements. We consider a linear N-element array with *half-wavelength* spacing, an angular field of view $[-\theta_{max}, \theta_{max}]$ for the array, where we set $\theta_{max} = \frac{\pi}{3}$ for a 120 degree sector. The channel from each mobile user to the base station is modeled as a line of sight (LoS) channel, but our insights apply more generally to sparse multipath channels with a dominant path. The fundamental bottleneck that we address in this paper is that, as we increase both the number of antenna elements and the bandwidth, the "narrowband assumption" for modeling the array response for a given user no longer applies, and the spatial channel for the user varies across the band.

M. Abdelghany, U. Madhow, and M. Rodwell are with the Department of Electrical and Computer Engineering, University of California at Santa Barbara, Santa Barbara, CA 93106 USA (e-mail: mabdelghany@ucsb.edu; madhow@ece.ucsb.edu; rodwell@ucsb.edu).

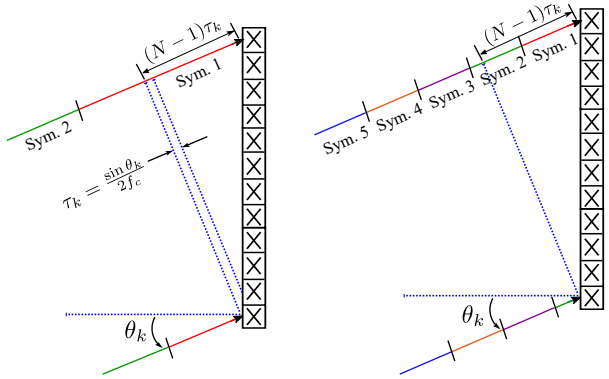

(a) Narrowband scenario. (b) Wideband scenario.

Figure 1: (a) Narrowband assumption holds, (b) Wideband modeling is required.

Specifically, the worst-case delay spread for a user across the array, normalized to the symbol period, is given by

$$\tau_D = BW\tau_{\max} \tag{1}$$

$$= \frac{BW}{2f_c} \times (N-1) \times \sin\theta_{\max}, \tag{2}$$

where BW denotes bandwidth (and hence symbol rate, ignoring excess bandwidth), f_c is the carrier frequency. The nominal system parameters we consider to illustrate our ideas are 140 GHz carrier frequency, 14 GHz bandwidth (10% of the carrier frequency), and $N = 256$, which yields a worst-case delay spread of about 11 symbols. On the other hand, if we reduced the bandwidth to as low as 200 MHz, the delay spread becomes 16% of a symbol, and the narrowband assumption is a good approximation. Fig. 1 provides a geometric illustration on when the narrowband assumption holds, and when wideband modeling must be used.

If we employ a standard multiuser detection strategy such as linear minimum mean square error (LMMSE) for spatial interference suppression based on nominal array responses at the center of the band, namely *narrowband LMMSE*, we can expect good performance in the scenario of Fig. 1 (a), and poor performance in that of Fig. 1 (b). This is illustrated by Fig. 2, which plots the BER attained with 5% outage in a picocell using narrowband LMMSE as a function of bandwidth. The performance is adequate for a small bandwidth of 200 MHz (worst-case delay spread of about 0.16 symbol), but deteriorates drastically by the time the bandwidth is increased to 1 GHz (worst-case delay spread of 0.8 symbol).

978-1-7281-0962-6/19/$31.00 ©2019 IEEE

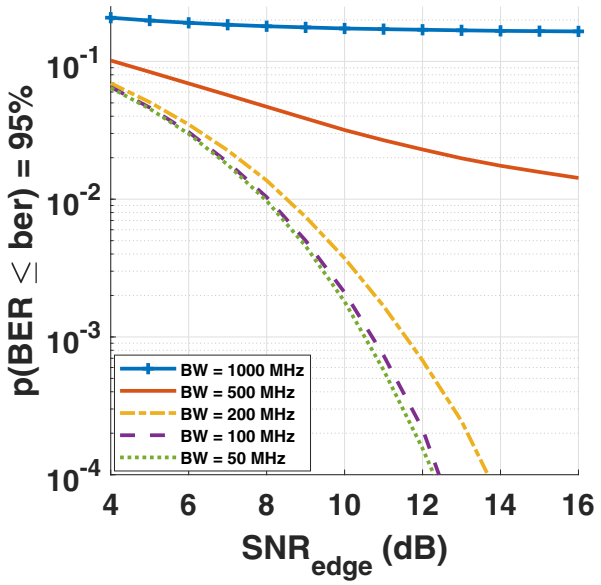

Figure 2: The figure shows the BER attained by 95% of the users if the narrowband LMMSE is used versus the SNR of the edge user at 100 m. The carrier frequency is 140 GHz and the base station is equipped with 256-element linear array.

A natural approach to address this problem is to employ MIMO-OFDM, a common strategy for lower carrier frequencies. For a large enough number of subcarriers, the narrowband assumption applies to each subcarrier, and we can perform per-subcarrier multiuser detection. While this has also been proposed for mmWave systems in a number of papers [1]–[4], there are two drawbacks to this approach. The first is the high Peak-to-Average Power Ratio (PAPR) of OFDM, which impairs power amplifier efficiency, already low in mm-wave systems with carrier frequencies above 100GHz. The second is that, since the spatial channels for the users are different over different subcarriers, one must employ a different spatial multiuser detection receiver for each subcarrier. This is potentially wasteful of computation, since it does not take advantage of the sparsity of the mmWave channel. In this paper, therefore, we consider single-carrier modulation, and exploit channel sparsity for the design of an efficient digital backend for wideband massive MIMO.

Related Work: For wideband single-carrier multiuser systems, there is general agreement in the literature on the strategy of dividing the spectrum of the received signal into smaller chunks and performing multiuser detection on each chunk separately, but there are variations in detail. In [5], the authors investigate a single-carrier frequency-domain equalization (SC-FDE) solution that employs LMMSE for MIMO processing. The authors of [6] combine SC-FDE with a time-domain decision feedback equalizer, along with interference cancellation. Since there is no channel structure assumed in [5] and [6] (the channel between each transmit and receive antenna element is modeled as multi-tap Rayleigh-fading), the LMMSE weights acquisition is complex.

In [7], the authors study the use of long arrays in LoS single-input multiple-output (SIMO) systems. They illustrate coupled signal dispersion in time and spatial frequency in the channel model, and design space-time receiver processing only over the dominant beams to reduce complexity. However, the problem of multiuser interference is not considered in [7]. In [8], the authors exploit the sparsity of the channel in both angular and delay domains to come up with channel estimation techniques which require less training overhead and have no pilot contamination. However, the paper does not address efficient multiuser detection.

Contributions: In this work, we address the problem of efficient multiuser detection in single-carrier wideband massive MIMO. Our benchmark is a signal-carrier frequency domain strategy, which may be interpreted simply as moving the inverse FFT in an OFDM transmitter to the receiver. Our main contribution is an alternative approach that exploits the sparsity of the received signal in the beamspace-frequency domain, which results from the sparsity of the spatial channel. Intuitively, transmitting over a wide band to a long array amounts to transmitting from a spread of spatial frequencies. In our proposed algorithm, we correct this spread by mapping it to fewer spatial frequencies. While the mapping does not completely remove the dependence of the channels on frequency, it dramatically reduces the variations, which in turn reduces the number of weights to be acquired for multiuser detection (e.g., by 16-fold compared to the benchmark approach for the parameters considered here).

Notation: We use lowercase bold letters for vectors, and uppercase bold letters for matrices. The notation $\mathbf{x} = [x_i]_{i=0}^{I}$ represents column vector $\mathbf{x}$ of length I and its elements are denoted by x_i. For a matrix, we use $\mathbf{X} = [x_{i,j}]_{i=0,j=0}^{I,J}$. If the size of the vector or the matrix can be inferred from the context, we write $\mathbf{X} = [x_{i,j}]_{i,j}$ for simplicity. $\{.\}_{k=1}^{K}$ denotes a list of K scalars, vectors or matrices.

II. System Model

The massive MIMO system comprises one base station and K single-antenna user terminals, as depicted in Fig. 3. The linear multiuser detector comprises two main blocks, the beamformer weights acquisition and the beamformer. The weights acquisition takes the spatial frequency of each mobile $\Omega_k = \pi \sin\theta_k$ and the noise variance σ^2 as inputs and generate the beamformer weights $\{\mathbf{w}\}_{i=1}^{K}$. After that, the beamformer uses these weights to estimate the mobiles' data vector $\mathbf{x}(t)$ out of the received vector $\mathbf{y}(t)$.

The time-domain received signal at the n^{th} antenna element in the base station, $y_n(t)$, can be expressed as

$$y_n(t) = \sum_{k=0}^{K-1} A_k x_k(t - n\tau_k) e^{-j2\pi n f_c \tau_k} + n_n(t), \qquad (3)$$

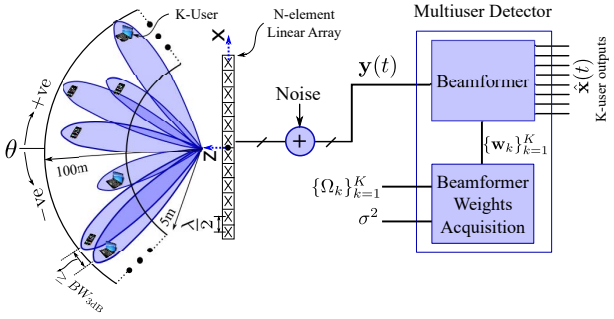

Figure 3: The cell size is constrained radially between 5 m and 100 m, and angularly between $-\pi/3 \leq \theta \leq \pi/3$. BW_{3dB} and $\hat{\mathbf{x}}(t)$ stand for the 3dB beamwidth the estimated data symbols vector. λ denotes the carrier's wavelength.

where $x_k(t)$ is a unit-variance time-domain symbols stream of the k^{th} user, $n_n(t)$ is band-limited complex white Gaussian noise process with variance σ^2, and $A_k^2 = \lambda^2/(4\pi R_k)^2$ depends on the radial location R_k of mobile k, using the Friis formula for path loss. f_c and λ are the carrier frequency and wavelength, and τ_k is the delay experienced by the k^{th} user's symbols stream between successive antenna elements. The delay $\tau_k = (\sin\theta_k)/(2f_c)$, $n \in [0, N)$, and $k \in [0, K)$. We assume that the pulse shape deployed in $x_k(t)$ is the sinc function.

A. Narrowband system

Here the delays τ_k are small compared to the symbol time, so that $x_k(t - n\tau_k) \approx x_k(t)$, and (3) can be written as

$$\mathbf{y}(t) = \mathbf{H}_{NB}\mathbf{x}(t) + \mathbf{n}(t), \tag{4}$$

where the received vector $\mathbf{y}(t) = [y_0(t), \ldots, y_{N-1}(t)]^\intercal$, the data symbols vector $\mathbf{x}(t) = [x_0(t), \ldots, x_{K-1}(t)]^\intercal$, the noise vector $\mathbf{n}(t) = [n_0(t), \ldots, n_{N-1}(t)]^\intercal$, the narrow-band channel matrix $\mathbf{H}_{NB} = [e^{-jn\Omega_k}]_{n,k}\mathcal{D}([A_k]_k)$, and $\mathcal{D}(.)$ is the diagonlization operator.

The LMMSE receiver is given by

$$\hat{\mathbf{x}} = \mathbf{W}_{NB}\mathbf{y}, \tag{5}$$

such that

$$\mathbf{W}_{NB} = (\mathbf{H}_{NB}^H\mathbf{H}_{NB} + \sigma^2\mathbf{I})^{-1}\mathbf{H}_{NB}^H. \tag{6}$$

B. Wideband system

Here, the delays τ_k can be larger than a symbol period. Taking the temporal Fourier transform $\mathcal{F}(.)$ for equation (3) yields

$$\begin{aligned}\tilde{y}_n(f) &= \sum_{k=0}^{K-1} A_k\tilde{x}_k(f)e^{-j2\pi n(f+f_c)\tau_k} + \tilde{n}_n(f) \\ &= \sum_{k=0}^{K-1} A_k\tilde{x}_k(f)e^{-jn(1+f/f_c)\Omega_k} + \tilde{n}_n(f),\end{aligned} \tag{7}$$

where $\tilde{y}_n(f) = \mathcal{F}(y_n(t))$, $\tilde{x}_k(f) = \mathcal{F}(x_k(t))$, and $\tilde{n}_n(f) = \mathcal{F}(n_n(t))$. This system of equations can be written in vector form as follows:

$$\tilde{\mathbf{y}}(f) = \tilde{\mathbf{H}}_{WB}(f)\tilde{\mathbf{x}}(f) + \tilde{\mathbf{n}}(f), \tag{8}$$

where the received vector in the frequency domain at the base station $\tilde{\mathbf{y}}(f) = [\tilde{y}_0(f), \ldots, \tilde{y}_{N-1}(f)]^\intercal$, the transmitted symbols stream in the frequency domain by the K users $\tilde{\mathbf{x}}(f) = [\tilde{x}_0(f), \ldots, \tilde{x}_{K-1}(f)]^\intercal$, the noise vector $\tilde{\mathbf{n}}(f) = [\tilde{n}_0(f), \ldots, \tilde{n}_{N-1}(f)]^\intercal$, and the wide-band channel matrix $\tilde{\mathbf{H}}_{WB}(f) = [e^{-jn(1+f/f_c)\Omega_k}]_{n,k}\mathcal{D}([A_k]_k)$.

The LMMSE solution at each frequency f is given by

$$\hat{\mathbf{x}}(t) = \mathcal{F}^{-1}(\tilde{\mathbf{W}}(f)\tilde{\mathbf{y}}(f)), \tag{9}$$

where

$$\tilde{\mathbf{W}}_{WB}(f) = \left(\tilde{\mathbf{H}}_{WB}(f)^H\tilde{\mathbf{H}}_{WB}(f) + \sigma^2\mathbf{I}\right)^{-1}\tilde{\mathbf{H}}_{WB}(f)^H \tag{10}$$

Practical digital signal processing methods must work with discretized system models, as discussed in the next subsection.

C. Signaling structure

Each mobile sends data in blocks of the length of M symbols. There is a guard interval of length L symbols between successive blocks to prevent Inter-Block Interference (IBI). Each guard interval is filled with a cyclic prefix to emulate a circular convolution. At the receiver, the base station discards the cyclic prefix and handles each data block separately. The sampled received signal can be written as

$$y_{n,m} = \sum_{k=0}^{K-1} A_k x_k(mT_s - n\tau_k)e^{-jn\Omega_k} + n_{n,m}, \tag{11}$$

where $T_s = 1/BW$ is the sampling time and BW is the bandwidth of the received signal, and $m \in [0, M)$.

III. Benchmark Wideband LMMSE

Fig. 4 illustrates the block diagram of the benchmark wideband LMMSE algorithm, which involves the following steps.

1) Temporal FFT: The discrete Fourier transform of equation (11) is given as follows,

$$\tilde{y}_{n,\ell} = \sum_{k=0}^{K-1} A_k\tilde{x}_{k,\ell}e^{-jn(1+\ell\frac{BW}{Mf_c})\Omega_k} + \tilde{n}_{n,\ell}, \tag{12}$$

where $[\tilde{x}_{k,-M/2}, \ldots, \tilde{x}_{k,M/2-1}] = \text{DFT}([x_k(\frac{m}{BW})]_m)$, DFT(.) is the discrete Fourier transform operation, and $\ell \in [-M/2, M/2)$. Given that $\tilde{\mathbf{y}}_\ell = [\tilde{y}_{n,\ell}]_n$, $\tilde{\mathbf{x}}_\ell = [\tilde{x}_{k,\ell}]_k$, and $\tilde{\mathbf{n}}_\ell = [\tilde{n}_{n,\ell}]_n$, the previous equation can be written in vector form as follows,

$$\tilde{\mathbf{y}}_\ell = \mathbf{H}(\ell)\tilde{\mathbf{x}}_\ell + \tilde{\mathbf{n}}_\ell, \tag{13}$$

where the channel matrix is given as

$$\mathbf{H}(\ell) = \left[e^{-jn(1+\ell\frac{BW}{Mf_c})\Omega_k}\right]_{n,k}\mathcal{D}([A_k]_k). \tag{14}$$

The temporal FFT divides the frequency domain of the received signal to M sub-band assuming that the channel is almost constant on the sub-band.

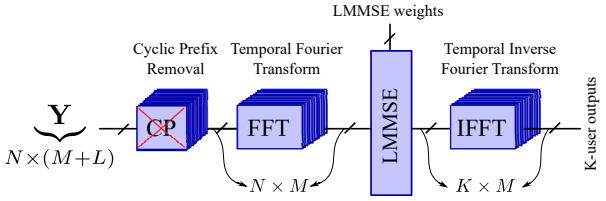

Figure 4: Block diagram for benchmark wideband LMMSE, where $\mathbf{Y}$ denotes the grid of received samples in antenna-space and time domain.

2) LMMSE Detection: In each sub-band, we can recall the narrowband assumption and detect $\tilde{\mathbf{x}}_\ell$ using LMMSE as follows,

$$\hat{\tilde{\mathbf{x}}}_\ell = \mathbf{W}(\ell)\tilde{\mathbf{y}}_\ell, \tag{15}$$

where

$$\mathbf{W}(\ell) = \left(\mathbf{H}(\ell)^H\mathbf{H}(\ell) + \sigma^2\mathbf{I}\right)^{-1}\mathbf{H}(\ell)^H. \tag{16}$$

3) Temporal IFFT: Finally, the receiver retrieves the data of the k^{th}user from the frequency-domain using temporal IFFT as $[\hat{x}_{k,0},\ldots,\hat{x}_{k,M-1}] = \text{IDFT}([\hat{\tilde{x}}_{k,\ell}]_\ell)$, where IDFT(.) is the inverse discrete Fourier transform operator. If the mobiles used OFDM instead of single carrier signaling, this step would have been already on the transmitter side.

IV. Proposed Wideband LMMSE

Fig. 5 delineates the block diagram of the proposed wideband LMMSE algorithm. The proposed algorithm is described in the following steps.

1) Temporal FFT: Similar to equation (13), the temporal FFT divide the bandwidth to M equally sub-bands. After this step, the conventional and proposed schemes start to differ.

2) Zero Padding and Spatial FFT: In this step, we aim to transform the received samples from the antenna-space to the beamspace with oversampling ratio O. So first, we pad the received samples vector per frequency bin $\tilde{\mathbf{y}}_\ell$ by a vector of zeros of size $(N(O-1))\times 1$. Then, we perform upon the spatial FFT as follows,

$$\breve{\mathbf{y}}_\ell = \text{DFT}([\tilde{\mathbf{y}}_\ell, \mathbf{0}_{N(O-1)}]^\intercal), \tag{17}$$

where $\mathbf{0}_M$ is vector of zeros of size $M\times 1$. Fig. 6 portrays the grid of the received samples power in beamspace-frequency-domain, i.e, $[|\breve{y}_{p,\ell}|^2]_{p,\ell}$, where $p\in[-\frac{NO}{2},\frac{NO}{2})$. This figure delineates the key idea of the proposed algorithm. As shown, each user is represented by a line that is governed by the equation $\Omega = \Omega_k(1+f/f_c)$, where Ω is the spatial frequency, and intersect the point $f=0$ and $\Omega=\Omega_k$. This can be inferred by the explicit expression of equation (17) which is given as follows,

$$\breve{y}_{p,\ell} = \sum_{k=0}^{K-1} A_k\tilde{x}_{k,\ell}c_{k,p,\ell}\frac{\sin(\frac{N}{2}(s_\ell\Omega_k+\frac{2\pi p}{NO}))}{\sin(\frac{1}{2}(s_\ell\Omega_k+\frac{2\pi p}{NO}))} + \breve{n}_{p,\ell}, \tag{18}$$

where $s_\ell = (1+\ell\frac{BW}{Mf_c})$, $c_{k,p,\ell} = \frac{1}{\sqrt{NO}}e^{-j\frac{(N-1)}{2}(s_\ell\Omega_k+\frac{2\pi p}{NO})}$, $\ell\frac{BW}{M}$ is the discretized version of f, $\frac{2\pi p}{NO}$ is the discretized version of Ω, and $\breve{n}_{p,\ell}$ is the noise element in the beamspace. The main idea of the proposed algorithm is to correct these tilted lines to make them horizontal. This is done by dividing the grid into multiple segments and correcting the slope of each segment, as shown in Fig. 7. Consequently, one LMMSE beamformer is adequate to retrieve all the data of a user per segment.

3) Slope Correction: We use linear interpolation to acquire the in-between points to correct the slope. We correct the slope by scaling p in equation (18), in that $\breve{y}_{p,\ell}$ becomes $\breve{y}_{p\frac{s_\ell}{s_x},\ell}$ where s_x corresponds to the frequency of the mid of the segment. We choose to work with linear interpolation due to its feasibility to be built in hardware.

4) Beamspace LMMSE Detection: In a segment, we use the channel corresponding to the mid of the segment to calculate the LMMSE solution for that segment. One can use efficient algorithm to do LMMSE detection in the beamspace as shown in [9].

5) Temporal IFFT: Finally, similar to the benchmark algorithm, the receiver retrieves the users' data from the frequency-domain using temporal IFFT.

Why the need for partitioning the data grid into multiple segments?

In slope correction process, the beam shapes get compressed or expanded. Fig. 8 depicts the beam shape of a single user after the data grid correction. Because the beam shape changes across the band, then one LMMSE beamformer is not adequate to retrieve the data from the entire band.

V. Results

The system setup is as illustrated in Fig. 3. The number of antennas is fixed at $N=256$ for all numerical experiments. In the simulations, the field of view is restricted to $-\pi/3\le\theta\le\pi/3$. The users are uniformly distributed inside a region bordered by a minimum and a maximum distance away from the base station, $R_{\text{min}}=5$ m and $R_{\text{max}}=100$ m, respectively. While the user terminals are placed randomly in our simulations, we enforce a minimum separation in spatial frequency between any two users in order not to incur excessive interference, arbitrarily choosing it as half the 3dB beamwidth: $\Delta\Omega_{\text{min}} = \frac{2.783}{N}$ [10]. We assume that users with similar spatial frequency can be served at different time. The number of users served simultaneously in the cell is 64 users, each is using QPSK modulation.

The carrier frequency of the system is $f_c = 140$ GHz and we choose to operate at bandwidth equals to 10% of f_c, i.e., 14 GHz. As can be inferred from Fig. 2, the narrowband assumption is inappropriate to use when dealing with such wide bandwidth and long array. The length of the cyclic prefix used $L = 2\times\lceil BW\times\tau_{\text{max}}\rceil = 24$ samples. We assume perfect CSI and no power control is deployed. The presented BER curves is plotted versus the SNR of the edge user at 100 m which is defined as $\text{SNR}_{\text{edge}} = NA_{100m}^2/\sigma^2$, where $N=256$ elements, and the channel strength at 100 m $A_{100}^2 = \lambda^2/(4\pi R_k)^2 = 0.002^2/(4\pi 100)^2$.

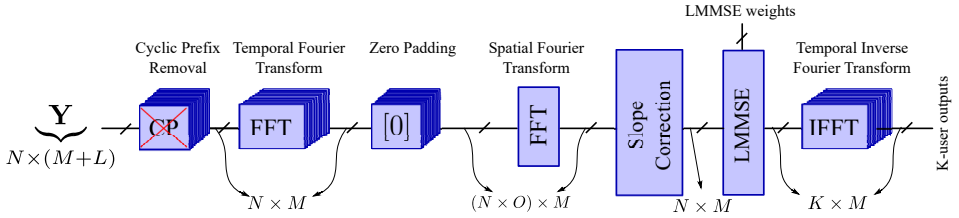

Figure 5: Block diagram of the proposed wideband LMMSE approach, where $\mathbf{Y}$ denotes the grid of received samples in antenna-space and time domain.

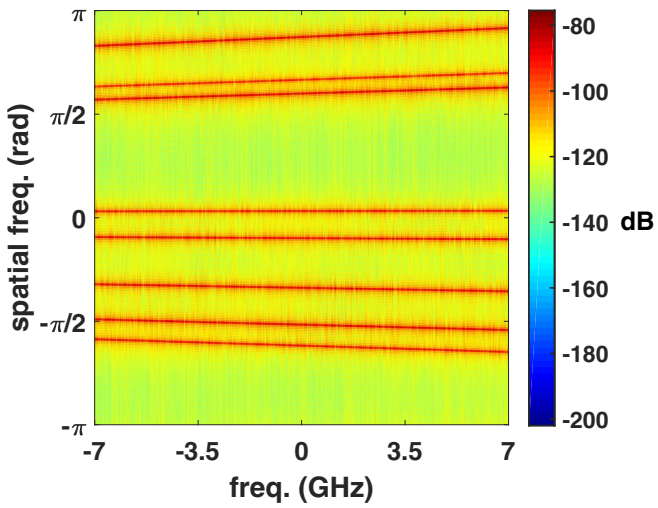

Figure 6: The beamspace-frequency-domain data grid before correction.

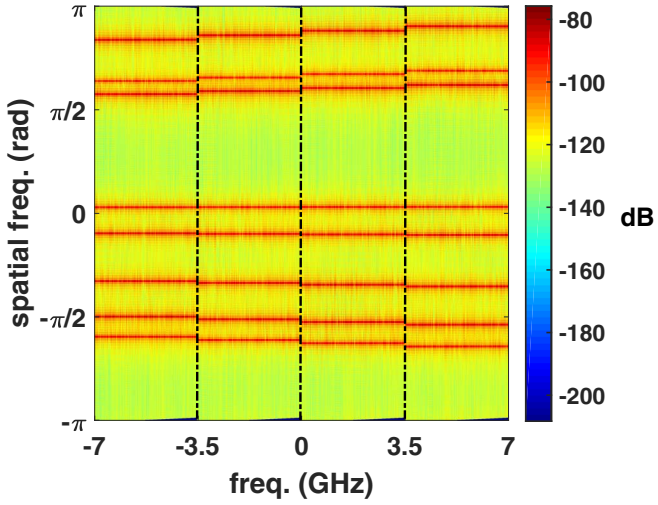

Figure 7: The beamspace-frequency-domain data grid after correction.

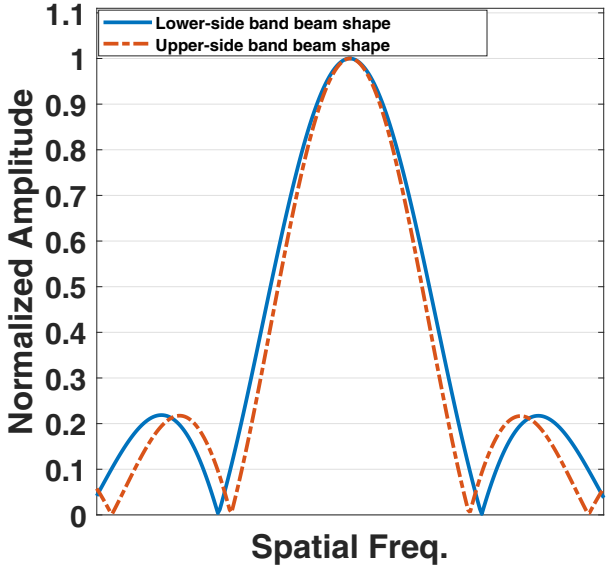

Figure 8: The beam shape of a single user after the grid correction.

A. *Benchmark Wideband LMMSE*

Fig. 9 shows the BER at 95% availability when the benchmark wideband LMMSE is employed. The benchmark algorithm is parameterized with the block length M, which determines the number of chunks into which the bandwidth is divided. As shown in the figure, a block length of 128 is enough to be within 1 dB of the baseline, defined for a system in which the narrowband assumption holds. Generally, what matters most is the maximum delay spread experienced by each sub-band not the block length itself. Using a block length of 128 symbols and bandwidth of 14 GHz, the maximum delay spread can be computed from equation (2) to be 9% of the symbol time.

B. *Proposed Wideband LMMSE*

Fig. 10 shows the BER at 95% availability for the proposed wideband LMMSE scheme. We choose the block length to be 256 to compensate for any additional errors introduced by

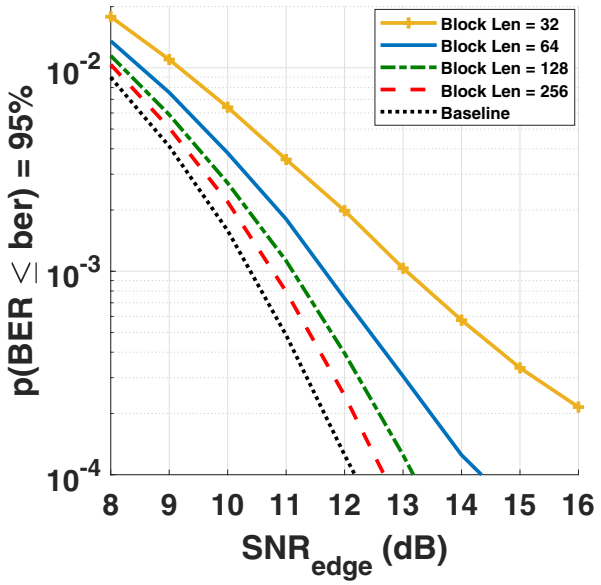

Figure 9: BER at 95% availability for the benchmark scheme with different block sizes.

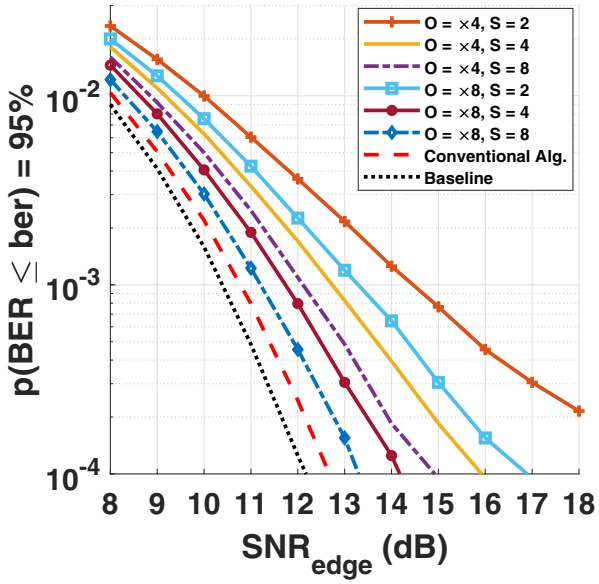

Figure 10: BER at 95% availability for the proposed wideband LMMSE for different settings and a block size of 256.

the proposed algorithm. O refers to the oversampling ratio in beamspace, and S denotes the number of segments used for beamspace partitioning. We use linear interpolation for simplicity. As shown in the figure, the proposed algorithm that uses an oversampling ratio of $O = 8$ and $S = 8$ yields a BER that is within 1 dB of the baseline. In contrast to the benchmark algorithm, which must learn a set of LMMSE weights per subband per user (i.e., 128 weight vectors per user), the proposed scheme only needs to learn 8 weight vectors per user. The price paid for simplifying the acquisition process is the increase in beamformer complexity due to an O times larger spatial FFT (the additional complexity due to linear interpolation is negligible).

VI. Conclusion

Our work shows that, as we push the limits of all-digital processing in scaling both bandwidth and spatial degrees of freedom, it is critical to exploit the characteristics of the mmWave channel to simplify processing. Specifically, we exploit the sparsity of the mmWave channel in this paper to drastically simplify the process of weights acquisition for frequency domain LMMSE (by 16-fold for the parameters considered here).

Acknowledgment

This work was supported in part by the Semiconductor Research Corporation (SRC) under the JUMP program (2018-JU-2778) and by DARPA (HR0011-18-3-0004). Use was made of the computational facilities administered by the Center for Scientific Computing at the CNSI and MRL (an NSF MRSEC; DMR-1720256) and purchased through NSF CNS-1725797.

References

[1] D. Zhu, J. Choi, and R. W. Heath, "Two-dimensional AoD and AoA acquisition for wideband millimeter-wave systems with dual-polarized MIMO," *IEEE Transactions on Wireless Communications*, vol. 16, no. 12, pp. 7890–7905, 2017.

[2] C. Mollen, J. Choi, E. G. Larsson, and R. W. Heath, "Uplink performance of wideband massive MIMO with one-bit ADCs," *IEEE Transactions on Wireless Communications*, vol. 16, no. 1, pp. 87–100, 2017.

[3] C. Studer and G. Durisi, "Quantized massive MU-MIMO-OFDM uplink," *IEEE Transactions on Communications*, vol. 64, no. 6, pp. 2387–2399, 2016.

[4] M. Wu, C. Dick, J. R. Cavallaro, and C. Studer, "High-throughput data detection for massive MU-MIMO-OFDM using coordinate descent," *IEEE Transactions on Circuits and Systems I: Regular Papers*, vol. 63, no. 12, pp. 2357–2367, 2016.

[5] J. Coon and M. Beach, "An investigation of MIMO single-carrier frequency-domain MMSE equalization," in *London Communications Symposium*, 9 2002, pp. 237–240.

[6] X. Zhu and R. D. Murch, "Novel frequency-domain equalization architectures for a single-carrier wireless MIMO system," in *Proceedings IEEE 56th Vehicular Technology Conference*, vol. 2, 2002, pp. 874–878.

[7] J. H. Brady and A. M. Sayeed, "Wideband communication with high-dimensional arrays: New results and transceiver architectures," in *IEEE International Conference on Communication Workshop (ICCW)*, 2015, pp. 1042–1047.

[8] B. Wang, F. Gao, S. Jin, H. Lin, and G. Y. Li, "Spatial-and frequency-wideband effects in millimeter-wave massive MIMO systems," *IEEE Transactions on Signal Processing*, vol. 66, pp. 3393–3406, 2018.

[9] M. Abdelghany, U. Madhow, and T. Antti, "Beamspace local LMMSE: An efficient digital backend for mmWave massive MIMO," in *IEEE 20th International Workshop on Signal Processing Advances in Wireless Communications (SPAWC)*, 2019.

[10] C. A. Balanis, *Antenna Theory: Analysis and Design*. New York, NY, USA: Wiley-Interscience, 2005.